Technical University of Denmark

DTU

The influence of wing twist on pressure distribution and flow topology

Kiefer, Janik; Sørensen, Niels N.; Hultmark, M; Hansen, Martin Otto Laver

DTU Library
Technical Information Center of Denmark

PAPER • OPEN ACCESS

The influence of wing twist on pressure distribution and flow topology

View the article online for updates and enhancements.

The influence of wing twist on pressure distribution and flow topology

J Kiefer[1], N N Sørensen [1], M Hultmark[2] and M O L Hansen[1]

[1] DTU Wind Energy, Technical University of Denmark, Kgs. Lyngby, Denmark
[2] Mechanical and Aerospace Engineering, Princeton University, Princeton, New Jersey, USA

E-mail: `jkie@dtu.dk`

Abstract. Empirical data serve as the foundation to computational modeling in the initial stages of the wind turbine design process. In case of aerodynamic simulations, the empirical input is comprised of lift and drag data obtained in quasi two-dimensional wind tunnel tests. In the simulations, the global flow over an entire blade is finally approximated as a spatial summation of the obtained 2-D data, which stands in strong contrast to the true operation of a wind turbine and consequently leads to a higher level of uncertainty. Especially, the near-root region of the blade experiences highly three-dimensional flow conditions, particularly in regions of the blade where the flow separates from the airfoil. This study aims to accentuate the difference between airfoil data obtained in quasi two-dimensional wind tunnel tests compared to airfoil data from a wing with an imposed three-dimensional spanwise pressure gradient. For this, a geometrically altered wing section with a spanwise twist is tested in a wind tunnel and compared to CFD computations.

1. Introduction
Before a wind turbine prototype is built and the final model goes into production, an iterative design process determines the basic layout of the turbine. Many different simulation techniques are utilized, which increase in their level of fidelity further into the process. The available computational power nowadays allows to carry out sophisticated and detailed flow (CFD) and structural analyses (FEM), which replicate real world aerodynamics and the corresponding loads in accurate detail. However, these simulation tools come among others with the drawback of higher computational cost, which limits their use to detailed improvements in the final stages of the design process before a first prototype of the wind turbine is built. In the case of CFD, the difficult prediction of stall onset depicts the main challenge to the computations.

High fidelity CFD and FEM simulations are preceded by engineering-type aero-elastic simulations, such as the Blade Element Momentum (BEM) algorithm in the first stage of the design optimization of a new wind turbine model. Semi-empirical data serve as the foundation to engineering-type simulations, which are thus heavily dependent on the accuracy of the provided data. In the case of aerodynamic simulations, the semi-empirical data are commonly comprised of two-dimensional lift and drag data of airfoil sections. Finally, a single blade of the turbine rotor is described as spatial summation of a finite number of airfoil sections. The airfoil sections are dimensioned with their respective geometric properties such as chord length and local twist angle, based on their corresponding lift and drag data. The global flow over the blade is thus approximated as the sum of multiple two-dimensional flows at the particular

airfoil sections. This assumption stands in strong contrast to the real-world application of a wind turbine and consequently leads to a higher level of uncertainty. To correctly model the flow over a wind turbine blade, one must consider that the turbine rotor is invariably located within the atmospheric boundary layer, in which turbulence and wind shear introduce unsteady and three-dimensional inflow conditions on the blade. Especially, the near-root region of the blade experiences highly three-dimensional flow conditions during the operation of the turbine [1], particularly in regions of the blade where the flow separates from the airfoil. The performance of present-day CFD and engineering-type simulations are only moderately satisfactory in correctly modeling said flow phenomena and continue to demand experimental validation data for improvement.

2. Work Objectives

The present study aims to elucidate and quantify the effect of an imposed three-dimensional pressure gradient on flow topology and pressure distribution of an airfoil. For this, wind tunnel tests on an airfoil section with an spanwise wing twist are carried out in conjunction with CFD simulations on the same geometry. Hereby, the study addresses one of the proposed research challenges listed in the aerodynamics section of reference [2], namely the potential extension from the two-dimensional airfoil concept to unsteady three-dimensional flow. In a simple first approximation towards a more realistic flow, this study aims to experimentally investigate the surface pressure distribution and hence lift and drag of a geometrically altered blade section in order to introduce a three-dimensional flow. A spanwise geometric twist of the airfoil section introduces a spanwise pressure gradient, whose strength is a function of the nominal angle of attack of the blade. The application of pressure taps allows in this study for the acquisition of the local pressure distribution at midspan of the airfoil section.

3. CFD Analysis

The in-house flow solver EllipSys3D is used for the CFD computations. The code is developed in co-operation between the Department of Mechanical Engineering and the Department of Wind Energy at Risø at the Technical University of Denmark, see [6, 7, 12]. The EllipSys3D code, is a multi-block finite volume discretization of the incompressible Reynolds Averaged Navier-Stokes (RANS) equations in general curvilinear coordinates. The code can use both multi-block matching grids, and overset grids as described in [14].

The convective terms, are discretized with the third order Quadratic Upstream Interpolation for Convective Kinematics (QUICK) upwind scheme [4]. The higher order schemes, are implemented using the deferred correction approach first suggested by Khosla and Rubin [3]. Central differences are used for the viscous terms, in each iteration only the normal terms are treated fully implicit, while the terms from non-orthogonality and the variable viscosity terms are treated explicitly.

In the present work the k-ω Shear Stress Transport (SST) eddy viscosity model [5] is used to model the boundary layer turbulence. The simulations are performed as transitional, predicting the laminar/turbulent transition on the wing by a E^n method, see [8]. The CFD grid is based on the original CAD geometry of the twisted blade, generating the surface grid in the commercial grid generator PointWise and the volume grid using the inhouse HypGrid3D, see [13]. The grid has 320 cells in the chord-wise direction, 128 cells in span-wise direction and 128 cells in normal direction. The span-wise extend of the domain is equal to 2.5 times the chord of the airfoil, and the farfield boundary are placed approximately 100 chords from the airfoil surface. The y^+ at the surface is kept below 1. The airfoil surface is specified as a no slip wall condition, symmetry conditions are applied in the spanwise directions, and at the farfield Dirichlet conditions are used for all the variables, except for a region +/- 45 degrees downstream of the airfoil where a zero gradient assumption is made.
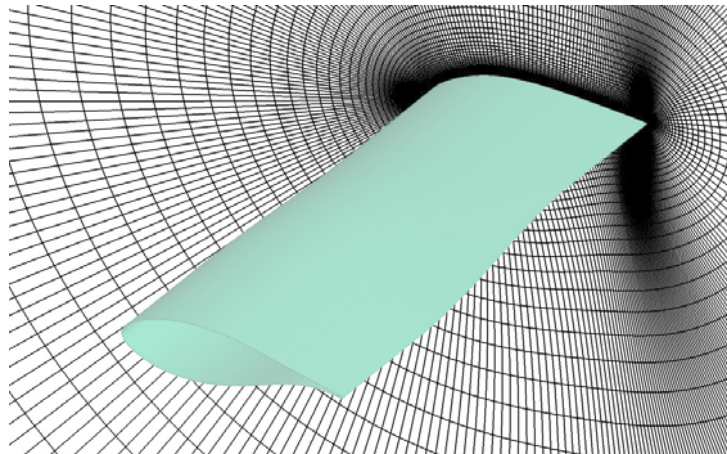
Figure 1. Grid in for computation of twisted airfoil in EllipSys3D.

4. Experimental Setup

The experiments in this study were performed at the Technical University of Denmark in an open-loop suction wind tunnel with a contraction ratio of $14:1$ leading to a $0.5 \times 0.5 \times 1.3 \ m^3$ test section. The laminar inflow is characterized by a turbulence intensity of $< 0.1\%$ for velocities ranging between $U_\infty = 0 - 65 \ m/s$. Static and total pressure of the inflow are measured with a Pitot static tube located at a distance of 2.5 chord lengths upstream of the airfoil leading edge in order to derive the undisturbed free-stream velocity. The acrylic glass test section is equipped with an in-house built single-component load cell, which measures the lift force perpendicular to the inflow direction by the internal excitation of metal-foil strain-gages. A wake rake with 32 active tubes, is installed 0.5 chord lengths downstream of the airfoil model at a height of $0.05 \ m$ above tunnel center line to capture the airfoil's wake.

The airfoil model is characterized by an underlying DU91-W2-250 profile of 25% relative thickness and an aspect ratio of $AR = 2.5$ spanning the test section vertically from test section floor to ceiling. The chord length of $0.2 \ m$ of the airfoil results in a high frontal area blockage of about $10 - 36\%$ for $0° \le \alpha \le 25°$. The pitch axis lies at the 1/4-chord. The geometric angle of attack is set during a measurement by a *JVL* MAC141-A1 brushless AC motor and controlled via a *Scancon* 2RHIF encoder with 9000 pulses per revolution resulting in an angle resolution of $\Delta\alpha = \pm 0.04°$.

As shown in figure 2 and compared to a commonly used 2D airfoil model, where the profile is uniformly extended over the length of the span, the present airfoil model features a geometric spanwise twist of $\theta = 10°$ about the quarter-chord axis. The twist introduces a non-linearly decreasing geometric angle of attack of $\Delta\alpha = 10°$, which follows a cosine function for values of $0 - \pi$ for a spanwise location of $0.25 \le y/S \le 0.75$ as shown in figure 3. The respective outboard regions of the airfoil each maintain a constant angle of attack to diminish potential wall interference influence on the spanwise pressure gradient. The airfoil is made from an ABS-polymer (acrylonitrile butadiene styrene) and was 3D-printed by means of the SLA (stereolithography) process in a spanwise buildup. 50 pressure taps are distributed in a straight line at mid-span on pressure and suction side of both airfoils. The airfoil was designed to include printed tubing inside the wings, which connect the surface pressure taps to outlets at the side of the wing. This made it possible to print the wing in one piece, rather than merging a top and bottom piece together after installing the pressure taps. Furthermore, it allows to handily connect the silicone tubes coming from the pressure sensor to the side of the wing. In this study only 32 out of the 50 taps were used and connected to a *Pressure Systems* 16TC/DTC pressure
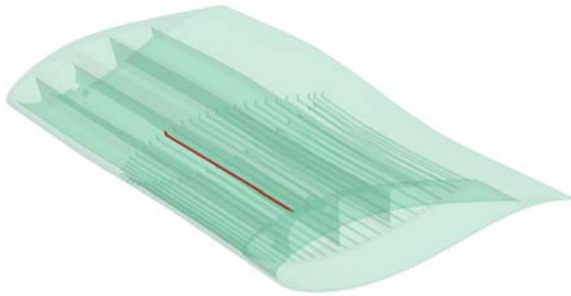
Figure 2. The 3D-printed and modified blade section with a non-linearly increasing twist angle. The embedded tubing connects 50 surface pressure taps at midspan to outlets on the left-hand side of the wing. One tube is highlighted in red.
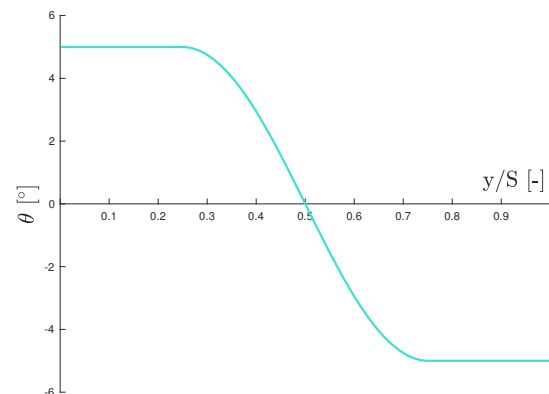
Figure 3. A geometric twist angle of $\Delta\theta = 10°$ is applied to the blade section. The twist distribution follows a cosine function for values from $0 - \pi$ for spanwise locations of $0.25 \leq y/S \leq 0.75$, where $y/S = 0$ is defined at the port-side of the wing.

sensor with a range of $\Delta p = \pm 1 \; psid$. An identical pressure sensor is used on the wake rake as well as for the free-stream Pitot static tube. The digital signal from the pressure sensors, as well as the amplified analog signal of the load cell were simultaneously sampled at $f_S = 330 \; Hz$ and recorded by NI Labview software, which was used for data acquisition.

5. Approach & Methods

The wind tunnel campaign was carried out at Reynolds numbers ranging from $0.2 \cdot 10^6 - 0.5 \cdot 10^6$ at angles of attack between $-10° \leq \alpha \leq +25°$, where the angle of attack is defined at mid span. This implies that the local angle of attack at the left-hand side of the wing is $-5°$ lower than the nominal angle of attack, and $+5°$ higher on the right-hand side. Except at the two turning points, data was acquired twice at every angle of attack in an upward and a downward pitching motion, respectively in order to monitor potential hysteresis effects. In order to check the repeatability of the experiments, runs were carried out three times at a chord based Reynolds number of $Re_c = 0.3 \cdot 10^6$. For the measured range of angles of attack, the maximum deviation of the lift coefficient was found to be $\Delta C_l = 0.010$ with a maximum angle deviation of $\Delta\alpha = 0.042°$ for the three repeated runs. Before solving the ring integral for the pressure distribution, two virtual pressure taps at the leading and trailing edge, oriented parallel to the chord were included in the calculation. The values of the surface pressures at these points were interpolated between the neighboring pressure taps.

6. Results

For quantitative comparison between experiment and CFD computations, figure 4 shows the pressure coefficient C_p plotted over the non-dimensionalized chord length x/c of the airfoil. Two computations were carried out in Ellipsys3D for transitional and fully turbulent flow, indicated as light green and dark green curves, respectively. The experimental data is shown as a blue curve with markers indicating the chordwise positions of the pressure taps on pressure and suction side of the airfoil. From left to right, the plots describe the pressure distributions at midspan of the twisted wing at geometric angles of attack of $\alpha = 5°, 10°$ and $15°$ at a constant

chord Reynolds number of $Re_c = 0.3 \cdot 10^6$. A positive C_p-value indicates suction, whereas a negative value describes surface pressures higher than the ambient static pressure.

Good agreement between the experiment and the computations can be observed for the pressure distribution on the pressure side of the airfoil for all angles of attack. Over the full range of angles of attack, the experiment and computations show the same relative locations of the stagnation point, which implies good accordance of the effective inflow angle in the experiment compared to the computations.

At $\alpha = 5°$, the turbulent flow case of the CFD computations exhibits slightly lower C_p-values, especially in the first half of the chord length. Yet, both CFD cases deviate from the experimentally obtained data, notably at chord lengths greater than $x/c = 0.5$. At a higher angle of $\alpha = 10°$, the deviation becomes larger and spreads from leading edge to regions close to the trailing edge. The turbulent CFD case shows a plateau in the pressure distribution starting from mid-chord, which could indicate fully separated flow past this point. The plateau is clearly evident for both CFD cases at a higher angle of attack of $\alpha = 15°$, as the onset of separation moves towards the leading edge. Though, the experimental data deviate from the CFD computations in C_p-value from the pressure peak up to $x/c = 0.6$, a similar plateau can be observed for the experiment from this point downstream. The C_p-value of the trailing edge pressure tap at $\alpha = 15°$ is an artifact from the pressure tap interpolation described in section 5 and shall be disregarded. The actual value is presumably close to the C_p-value at $x/c = 0.8$.
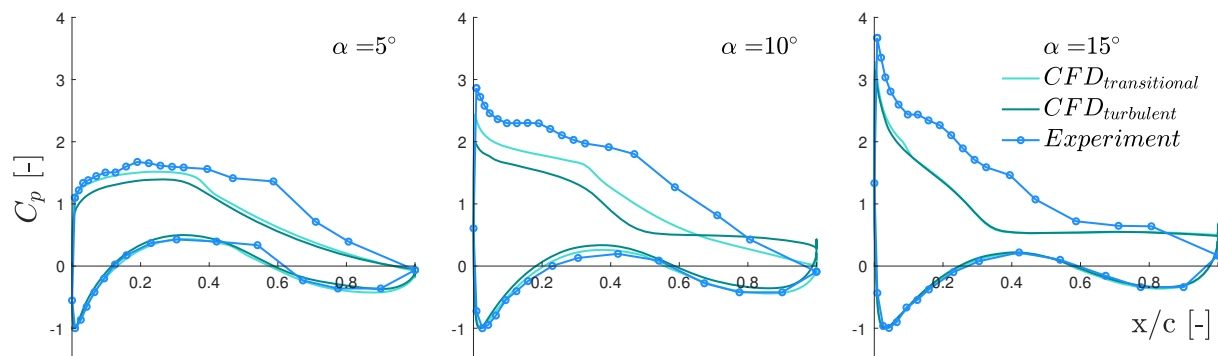
Figure 4. The pressure coefficient C_p plotted over the non-dimensionalized airfoil chord length x/c for comparison between experiment and two CFD computations in Ellipsys3D of transitional and fully turbulent flow. Plots are shown for angles of attack of $\alpha = 5°, 10°, 15°$ at a constant chord Reynolds number of $Re_c = 0.3 \cdot 10^6$. Legend and axis labels are valid for all three plots.

In order to obtain a qualitative insight to the flow structure at the airfoil surface, the airfoil model was later equipped with 72 red tufts, each 2.5 cm in length. The tufts were distributed in an uniform pattern at relative distances of 3 cm in the chordwise and 2 cm in the spanwise direction. Despite the presumable influence of the tufts on each other, the pattern was chosen to be rectangular in an attempt to visualize the contorted surface of the wing. The flow goes from left to right in figure 5, which shows the airfoil model mounted in the wind tunnel test section at different angles of attack. The images show the airfoil suction side and were taken at constant $Re_c = 0.3 \cdot 10^6$ with a shutter speed of $1/50$ of a second. The relatively low shutter speed allows unsteady and fast moving tufts to appear blurry and indicate a region of unsteady and turbulent flow. From left to right, the images were taken at geometric angles of attack of $\alpha = 5°, 10°$ and $15°$, which depict the angle at mid span at location of the pressure taps. The pressure taps are indicated by black "+"-markers. A white dotted line approximates the
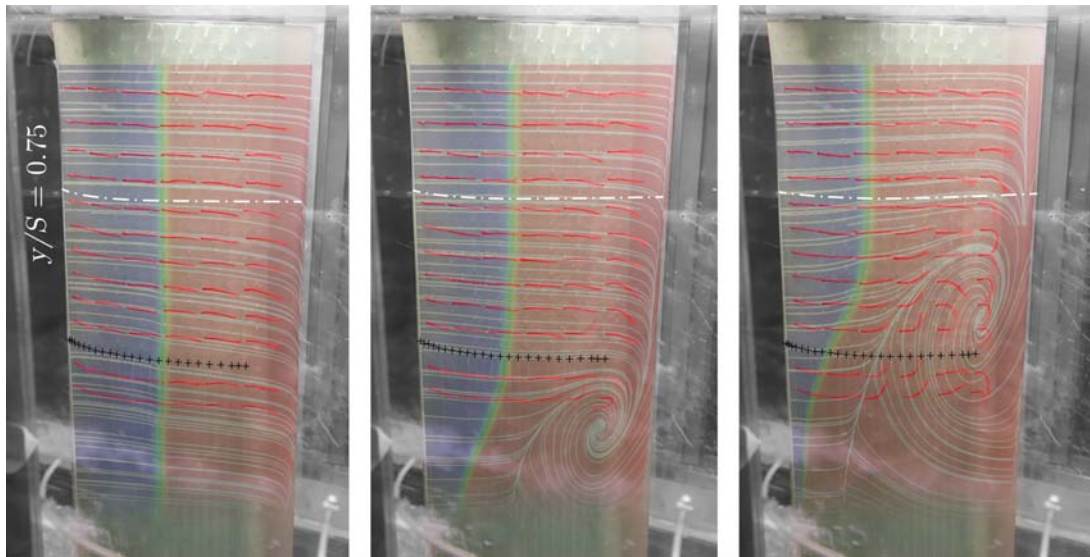
Figure 5. The pictures from left to right show the twisted wing in the wind tunnel test section at geometric angles of attack of $\alpha = 5°, 10°$ and $15°$ at a constant Reynolds number of $Re_c = 0.3 \cdot 10^6$. For qualitative comparison the images are overlaid with plots of limiting streamlines extracted from EllipSys3D for the transitional flow case. Tufts applied to the blade section are red, the laminar flow region of the CFD output is shown in blue and the turbulent flow region in red. The locations of the pressure taps are illustrated with black "+"-markers. Flow goes from left to right.

spanwise location of $y/S = 0.75$, at which the twist angle reaches its minimum of $\theta = -5°$ and remains constant from there outwards. In the orientation of the images, the local angle of attack is therefore highest at the bottom of the picture and lowest at the top.

The pictures taken in the experiment were manually overlaid with flow visualization images obtained from the CFD computation, in which blue and red indicate regions of laminar or turbulent flow, respectively. The computed laminar to turbulent transition is illustrated in green, while limiting streamlines are plotted in white.

The comparison illustrates good qualitative agreement of the flow topology between the experiment and the CFD computation for all angles of attack shown. At the lowest angle of $\alpha = 5°$, the flow near the trailing edge bends slightly downwards towards spanwise sections at higher local angle of attack and thus lower pressures.

Surprisingly and despite the relatively high spanwise twist of $\theta = 10°$ over only 1.25 chord lengths, this phenomenon appears solely close to the trailing edge, whereas the majority of the wing exhibits a steady two-dimensional flow approximately perpendicular to the leading-edge. With increasing nominal angles of attack and as the high-α side of the wing begins to stall, the flow becomes highly three-dimensional.

At $\alpha = 10°$, the CFD computations predict the development of a clockwise-turning swirling pattern indicated by the limiting streamlines and presumably located in between regions of separated and attached flow. The tufts show good agreement with the anticipated flow topology in terms of orientation and unsteadiness. Near the core of the swirling pattern, the tufts are heavily blurred due to high fluctuations in the flow direction, whereas tufts further away are steadily oriented. With further increase of the angle of attack to $\alpha = 15°$, the swirling pattern moves towards the low-α side of the wing and the plotted streamlines as well as the tufts bend more. The size of the swirling pattern increases and indicates a large area of separated flow.

The flow bending downwards near the trailing edge or the flow deflection angle, respectively becomes greater with increasing angle of attack.

7. Conclusion

To investigate the effects of a spanwise pressure gradient on a three-dimensional wing, a blade section based on the DU91-W2-250 profile with constant chord length but a spanwise twist of $\theta = 10°$ was 3-D printed including pressure taps at midspan. The blade section was mounted in a wind tunnel and the chordwise pressure distribution was measured for Reynolds numbers between $0.2 \cdot 10^6$ and $0.5 \cdot 10^6$ at angles of attack between $-10°$ and $25°$, where the angle of attack is defined at the midspan. In parallel the same geometry was modeled using CFD, in which the overall flow was not confined by wind tunnel walls.

Simulations and experiment indicate a complex 3-D flow topology, especially when the inflow angles become high enough for the boundary layer to separate at the high-α side of the blade section. The qualitative comparison between the orientation of applied tufts in the experiment and limiting streamlines extracted from the computations yields good agreement. However, the direct comparisons between the measured and computed chordwise pressure distributions at midspan for the high angles of attack of $10°$ and $15°$ show a quite large discrepancy and the reason is not yet fully understood. The discrepancy could be caused by the absent wind tunnel walls in the CFD simulations, where the bending of the streamlines is less restricted compared to the experiment. Additionally, blockage effects and the thereby caused probable speed-up between the blade section and the tunnel walls may potentially emphasize the observed error. Furthermore, the combination of an enforced 3-D stall on a relatively thick airfoil $t/c = 25\%$ may be a hard case to model, utilizing two equation turbulence models such as the $k - \omega$-type models applied in this study.

For future computations it is intended to include the wind tunnel walls and deploy improved CFD strategies such as Delayed Detached Eddy Simulations (DDES) with Improved wall-modeling capability (IDDES). These methods are computationally more expensive but are likely to obtain improved results.

8. Future Work

It is planned to test the hypotheses proposed in section 7, namely the addition of wind tunnel walls to the CFD computations and the reduction of blockage effects in the experiment in a subsequent study. The latter will be achieved with a new wind tunnel test section of 1.5 times the current width, which is presently being built. Furthermore, it is intended to gauge the dimensions of the 3D-printed model in high resolution, in order to assess potential deviations from the CAD model due to shrinking or warping following the printing process.

Ultimately, the aim is to experimentally obtain the global surface pressure of the three-dimensional blade section by the application of pressure sensitive paint. This will allow for the acquisition of pressure maps in high temporal and spatial resolution in the chordwise and spanwise direction. The results will enable a detailed insight in the fundamental influence of twist on the three-dimensional surface pressure distribution of the airfoil and may serve as a test case for CFD computations.

References

[1] Herráez I et al 2014 Insight into Rotational Effects on a Wind Turbine Blade Using Navier-Stokes Computations *Energies* 7 6798-6822 doi:10.3390/en7106798

[2] Van Kuik G and Peinke J 2016 Long-term research challenges in wind energy a research agenda by the European academy of wind *Springer* doi: 10.1007/978-3-319-46919-5

[3] P. K. Khosla and S. G. Rubin. A diagonally dominant second-order accurate implicit scheme. *Computers Fluids*, 2:207–209, 1974.

[4] B. P. Leonard. A stable and accurate convective modelling procedure based on quadratic upstream interpolation. *Comput. Meths. Appl. Mech. Eng.*, 19:59–98, 1979.

[5] F. R. Menter. Zonal Two Equation k-ω Turbulence Models for Aerodynamic Flows. *AIAA paper 1993-2906*, 1993.

[6] J. A. Michelsen. Basis3D - a Platform for Development of Multiblock PDE Solvers. Technical Report AFM 92-05, Technical University of Denmark, Department of Fluid Mechanics, Technical University of Denmark, December 1992.

[7] J. A. Michelsen. Block structured Multigrid solution of 2D and 3D elliptic PDE's. Technical Report AFM 94-06, Technical University of Denmark, Department of Fluid Mechanics, Technical University of Denmark, May 1994.

[8] J. A. Michelsen. *Forskning i aeroelasticitet EFP-2001*, chapter Beregning af laminar-turbulent omslag i 2D og 3D, page 73. Risø-R1349(DA). 2002. In Danish.

[9] S. V. Patankar. *Numerical Heat Transfer and Fluid Flow.* Hemisphere Publishing Corporation, 1980. ISBN: 0891165223.

[10] S. V. Patankar and D. B. Spalding. A Calculation Prodedure for Heat, Mass and Momentum Transfer in Three-Dimensional Parabolic Flows. *Int. J. Heat Mass Transfer*, 15:1787, 1972.

[11] C. M. Rhie. *A numerical study of the flow past an isolated airfoil with separation.* PhD thesis, Univ. of Illinois, Urbana-Champaign, 1981.

[12] N. N. Sørensen. General Purpose Flow Solver Applied to Flow over Hills. Risø-R- 827-(EN), Risø National Laboratory, Roskilde, Denmark, June 1995.

[13] N. N. Sørensen. HypGrid2D a 2-D Mesh Generator. Risø-R- 1035-(EN), Risø National Laboratory, Roskilde, Denmark, Feb 1998.

[14] F. Zahle. *Wind turbine aerodynamics using an incompressible overset grid method.* PhD thesis, 2006.